Carbohydrate Polymers 207 (2019) 169–179

Contents lists available at ScienceDirect

Carbohydrate Polymers

journal homepage: www.elsevier.com/locate/carbpol

Banana starch nanocomposite with cellulose nanofibers isolated from banana peel by enzymatic treatment: *In vitro* cytotoxicity assessment

H. Tibolla[a,*], F.M. Pelissari[b], J.T. Martins[c], E.M. Lanzoni[d,e], A.A. Vicente[c], F.C. Menegalli[a], R.L. Cunha[a]

[a] Department of Food Engineering, School of Food Engineering, University of Campinas, Campinas, SP, CEP 13083-862, Brazil
[b] Institute of Science and Technology, Food Engineering, University of Jequitinhonha and Mucuri, Diamantina, MG, CEP 39100-000, Brazil
[c] CEB – Centre of Biological Engineering, University of Minho, 4710-057, Braga, Portugal
[d] Brazilian Nanotechnology National Laboratory (LNNano), Brazilian Center for Research in Energy and Materials (CNPEM), 13083-970, Campinas, SP, Brazil
[e] São Paulo State University (UNESP), Institute of Science and Technology, Sorocaba, Brazil

ARTICLE INFO

Keywords:
Starch composite
Cellulose nanofibers
Enzymatic hydrolysis
Nanofiber cytotoxicity

ABSTRACT

The potential use of cellulose nanofibers (CNFs) as a reinforcing agent in banana starch-based nanocomposite films was investigated. CNFs were isolated from banana peel (*Musa paradisiaca*) by enzymatic hydrolysis. Banana starch-based nanocomposite films were prepared with CNFs using the casting method. CNFs effect on cell viability and on nanocomposite films properties' was investigated. The cytotoxicity of CNFs was assessed on Caco-2 cell line. CNFs were not cytotoxic at 50–2000 μg/mL. However, CNFs above 2000 μg/mL significantly decreased cell viability. Topography analysis showed that the incorporation of CNFs modified the film structure. The nanocomposites exhibited a complex structure due to strong interactions between CNFs and starch matrix, promoting a remarkable improvement on mechanical and water barrier properties, opacity and UV light barrier compared to the control film. CNFs can offer a great potential as reinforcing material for starch-based nanocomposite films, producing a value-added food packaging from a waste material.

1. Introduction

The increasing demand for environmentally friendly products and processes has encouraged the efficient exploitation of new biopolymers, such as cellulose, which is the most abundant renewable polymer available on the earth. The agricultural practice generates a considerable amount of residues rich in cellulose and its recovery adds value to this by-product, besides contributing to the reduction of environmental pollution. Bananas are an important food crop that is extensively grown in tropical and subtropical regions. Usually, banana peel, rachis, leaves and rhizome are by-products of banana processing in the food industry and can be an alternative source of natural bioactive compounds (*e.g.*, fibers) (Padam, Tin, Chye, & Abdullah, 2014). Especially, banana peel contains a considerable amount of cellulose (12%) and this material can be potentially applicable as a reinforcing component in high-performance composite films (Elanthikkal, Gopalakrishnapanicker, Varghese, & Guthrie, 2010; Tibolla, Pelissari, Rodrigues, & Menegalli, 2017). Simultaneously to numerous research studies for biodegradable composite films production, cellulose microfibrils and CNFs from banana by-products (*e.g.*, rachis and peel) have been explored as an alternative to reinforce polymeric matrices (Gómez et al., 2012; Padam et al., 2014; Zuluaga, Putaux, Restrepo, Mondragon, & Gañán, 2007). CNFs show several advantages, for instance, their potential to improve the thermal stability, mechanical and barrier properties (water vapor and oxygen permeability), besides being a biodegradable and renewable source (Andrade-Mahecha, Pelissari, Tapia-Blácido, & Menegalli, 2015; Pelissari, Andrade-Mahecha, Sobral, & Menegalli, 2017).

The CNFs production from lignocellulosic source involves a series of processes. Currently, different methods for cellulose nanofibril isolation have been developed. Chemical hydrolysis, such as acid treatment and catalytic oxidation, is performed to separate the cellulose fibrils from the cell wall. On the other hand, enzymatic hydrolysis is a method that gained prominence over the last decade, which has several advantages compared to the chemical methods (*e.g.*, it does not involve the use of chemical reagents). Thus, it can be considered an environmentally friendly process. Our previous studies showed that enzymatic treatment successfully isolates CNFs from the banana peel (Tibolla et al., 2017).

The growing interest in nanotechnology area leads to a subsequent increase of the population exposure to nanomaterials. Thus, it is essential to assess the possible effects, benefits and risks of these

* Corresponding author.
E-mail address: heloisatibolla@gmail.com (H. Tibolla).

https://doi.org/10.1016/j.carbpol.2018.11.079
Received 23 May 2018; Received in revised form 20 November 2018; Accepted 23 November 2018
Available online 24 November 2018
0144-8617/

nanomaterials to the human health (Clift et al., 2011). The development of toxicological analysis is vital in the biodegradable films production, since there is a high possibility that nanomaterials migrate from the packaging material into foods and consequently, ingested by humans (Lima et al., 2012). Currently, Caco-2 cell line (human colon adenocarcinoma origin) is the most popular *in vitro* model for toxicological evaluation of the nanomaterials since the cells structural and functional performance (*e.g.*, absorption) are similar to small intestinal enterocytes (Antunes, Andrade, Araujo, Ferreira, & Sarmento, 2013; Jones & Grainger, 2009). Presently, there are few reports in the literature regarding to CNF cytotoxicity assessment (Alexandrescu, Syverud, Gatti, & Chinga-Carrasco, 2013; Pereira et al., 2013). This is partially due to the fact that CNFs are derived from bio-based sources suggesting that the material could be used without significant health concern. Besides, the cellulose degradation does not normally occur in the human body (Antunes et al., 2013; Clift et al., 2011; Moreira, 2009). Nevertheless, *in vitro* studies, already reported that CNFs potentiated inflammatory responses. Pereira et al. (2013) evaluated cotton CNFs *in vitro* cytotoxicity using mammalian fibroblasts. The authors observed that under high concentrations (2000 μg/mL), CNFs caused a decrease in cell viability up to 36.51%.

This work aimed at studying an agricultural waste (banana peel) as raw material for preparing high added value products. The potential use of CNFs, obtained from banana peel by enzymatic treatment, as reinforcing agent in biopolymer composite films was investigated. The CNF safety and biocompatibility were firstly evaluated by cell viability measurements. Consequently, the produce banana starch-based nanocomposite films with CNFs incorporated were characterized in terms of mechanical, barrier, optical, chemical and structural properties.

2. Material and methods

2.1. Materials

The fruit, unripe banana from variety "Terra" (*Musa paradisiaca*), was obtained from the southeastern region of Brazil. The banana fruit was not subjected to any postharvest treatment. The starch was isolated from unripe plantain bananas according to the methodology described by Pelissari, Andrade-Mahecha, Sobral, and Menegalli (2012). The extracted banana starch reached a purity of 94.8%; 50.3, 35.0 and 1.0% (in dry basis) corresponded to resistant starch, amylose and protein, respectively. CNFs were isolated from banana peel by enzymatic hydrolysis using xylanase, according to the method described by Tibolla et al. (2017). Xylanase was kindly provided by Novozymes (Araucária – PR, Brazil). The authors performed previous experimental tests to select the best enzymatic hydrolysis conditions, in order to improve CNFs properties that were used as reinforcing agent of polymeric matrices. CNF1 and CNF2 were obtained by enzymatic hydrolysis using different banana peel bran concentration and temperature conditions. Banana peel bran at 15% (CNF1 treatment) or 35% (CNF2 treatment) and 0.1 M acetate buffer (pH 6.0) were placed in the thermostatic shaker at 35 °C (CNF1 treatment) or 55 °C (CNF2 treatment) for 10 min. Then xylanase at 70 U/g was added to the mixture and left at the desired temperature for 24 h, under agitation (150 rpm). The suspensions were placed in a thermostatic bath at 80 °C for 30 min to denature the enzyme. Then the residual pulp was washed with deionized water, the solid was centrifuged during 15 min at 10,000 rpm (5 °C) and suspended in deionized water to obtain CNF1 and CNF2 samples. Table 1 summarizes the characteristics of the two CNFs (CNF1 and CNF2) used in this study. The Caco-2 cell line (American Type Culture Collection (ATCC)) used on CNFs cytotoxicity evaluation was kindly provided by Professor Doutor Bruno Sarmento, Instituto Superior de Ciências da Saúde – Norte (Porto, Portugal). All cell culture reagents were purchased from Gibco™ Invitrogen, Sigma and Lonza. All the chemicals used in this work were reagent grade.

2.2. CNF effect on cell viability

2.2.1. Cell culture

Human colon carcinoma Caco-2 cell line was used at passages 22–29 (i.e., number of times the culture has been subcultured). Caco-2 cells were grown in culture flasks containing Dulbecco's Modified Eagle Medium (DMEM) supplemented with 10% (v/v) heat inactivated fetal bovine serum, 1% (v/v) L-glutamine, 1% (v/v) non-essential amino acids and 1% (v/v) penicillin-streptomycin, and incubated at 37 °C under 5% CO_2 water saturated atmosphere. After cells achieving approximately 90% of confluence, the cells were harvested from flasks with trypsin. The number of viable cells in suspension was estimated by counting in a Neubauer chamber with an inverted microscope.

2.2.2. Cell viability assay

CNFs effect on cell viability was assessed using methylthiazolyldiphenyl-tetrazolium bromide (MTT) conversion assay. CNFs were prepared at selected concentrations (50, 100, 500, 1000, 2000 and 5000 μg/mL) in supplemented DMEM medium and homogenized. Caco-2 cells suspension was seeded in 96-well microplate (at 2.5×10^5 cells/mL), in 200 μL of supplemented DMEM and incubated for 24 h at 37 °C under a 5% CO_2 environment. Then, medium was changed, and CNFs test solutions were added to the cell culture and incubated (37 °C; 5% CO_2) for 24 h. A blank sample (DMEM without cells) and a positive control (DMEM with cells) were also tested. Each treatment was tested in quadruplicate. Thereafter, the supernatant was removed and 200 μL of MTT solution (0.5 mg/mL in DMEM supplemented) was added to each well, protected from the light, and incubated at 37 °C for 4 h, to allow the formation of purple formazan crystal. Afterward, the medium was removed, and purple formazan crystals were solubilized from cells using 200 μL of DMSO. The culture plates were shaken on an orbital shaker for 30 min in order to completely solubilize purple formazan crystals. The enzymatic reduction of yellow tetrazolium MTT to a purple formazan was measured by Synergy™ HT Multi-mode Microplate Reader (Biotek Instruments, Winooski, VT, USA) at 570 nm and 690 nm, the latter was used for background subtraction. Cell viability (%) was calculated using Eq. (1).

$$\text{Cell viability}\,(\%) = \frac{A_{Exp} - A_{control}}{A_{positive} - A_{control}} \times 100 \quad (1)$$

where: A_{Exp} is the absorbance of CNFs (CNFs solution + cell) sample; $A_{control}$ is the absorbance value of blank (DMEM without cell) sample; $A_{positive}$ is the absorbance value of positive control (DMEM + cell).

2.3. Nanocomposite films production

The banana starch films were produced by the casting method according to the methodology adapted from Pelissari et al. (2017). The first step involved the dispersion of CNF suspension (5 g of nanofibers/100 g of starch) by magnetic stirring for 15 min, followed by homogenization with an Ultra-Turrax (5000 rpm for 15 min). The CNF suspension was added to a water solution containing 4% (w/w, dry basis) of banana starch previously stirred for 30 min. The mixture was homogenized by mechanical stirring for 30 min, followed by heating up to 81 °C under gentle stirring. Glycerol (25 g of glycerol/100 g of starch) was added at this point, and the solution was maintained at this temperature for 15 min. After that, the film-forming suspension (FFS) was sonicated for 10 min and 70.4 g of the FFS was poured onto acrylic plates (18 × 21 cm) to control the thickness of the nanocomposite films. The films were dried in a chamber with air circulation under controlled temperature (54 °C) and relative humidity (RH) (48%) for 4 h. A film without added CNFs (control) was produced for comparison purpose. The films were conditioned in desiccators under 58% RH, at 25 °C, for 48 h for further film characterization. The produced films were named as control film without CNFs (CF); films containing 5% (w/

Table 1
Characteristics of cellulose nanofibers (CNFs) added to starch-based films.
Data from Tibolla et al.2017).Table 1.

Film	CNFs	CNFs characteristics				
		Length (L)[a] (nm)	Diameter (d)[a] (nm)	Aspect ratio (L/d)	ζ-potential (mV)	Crystallinity index (%)
CNFF1	CNF1	1490.0 ± 107.3	3.7 ± 0.4	404.5 ± 63.9	−29.1 ± 0.7	61.5 ± 1.1
CNFF2	CNF2	1544.5 ± 40.6	8.8 ± 0.7	170.2 ± 14.7	−31.5 ± 2.9	66.2 ± 4.1

CNFF1: nanocomposite films reinforced with CNF1 cellulose nanofibers; CNFF2: nanocomposite films reinforced with CNF2 cellulose nanofiber.
[a] The CNF diameter was determined by atomic force microscopy (AFM) image analysis. Dynamic light scattering (DLS) technique can be considered as a helpful tool to compare nanofibers in terms of relative size trends among a series of preparations. In the case of produced cellulose nanofibers, the DLS values measured may give an approximate estimation of nanofibers length; however, a precise length value is not possible to detect using this technique.

w) of CNF1 (CNFF1) and films containing 5% (w/w) of CNF2 (CNFF2).

2.4. Nanocomposite films characterization

2.4.1. Topography and roughness

The topography and roughness of the films was analyzed by scanning electron microscopy (SEM) and atomic force microscopy (AFM) techniques. To perform the analysis, a piece of film (10 × 10 mm) was dehydrated in a desiccator containing silica gel (~0% RH) for 3 weeks. For the SEM analysis, the dried film samples were fractured with the help of tweezers, and small fragments were obtained. Fragment samples were fixed on aluminum stubs with a double-sided tape and then, they were coated with a layer of gold (Sputter Coater POLARON, model SC7620), to improve conductivity. The coated samples were observed under a scanning electron microscope (LEO, model LEO 440i, Cambridge, England) operating at an acceleration voltage of 15 kV. AFM analysis was performed in an Nx-10 Atomic Force Microscope (Park systems, Suwon, Korea). The sample, previously dehydrated, was placed on a grid with mica surface. The digital images were acquired under controlled environmental conditions (RH ≤ 10% and 25 °C). The morphology and roughness of the films were analyzed by image analysis using the Gwiddion software (version 2.44).

2.4.2. Thickness, density and moisture content

Film thickness was measured using a digital micrometer (Digimatic Micrometer Series 293 MDC-Lite, Mitutoyo Corporation, Japan) with an accuracy of 0.001 mm. The mean thickness of each film was determined from an average of ten random measurements.

To determine film density, 20 × 20 mm squares samples were cut and their thickness was measured (three random measurements). The film samples were weighted. The density of the films was calculated as the ratio between the film weight and film volume (film thickness × film area). The density experiments were performed in triplicate, and the data were reported as mean values.

The film moisture content was analyzed according to gravimetric method, in triplicate, by drying the samples at 105 °C for 24 h (AOAC, 2005).

2.4.3. Mechanical properties

The film mechanical properties were investigated using a texture analyzer (Stable Micro Systems, model TA.TXplus, Surrey, UK, England), according to the standard method D882-12 (ASTM, 2012). An average of six determinations was performed for each film sample. The samples were cut into 20 × 80 mm strips with a scalpel. The initial grip separation and crosshead speed were set at 40 mm and 1.0 mm/s, respectively. The tensile strength (force/initial cross-sectional area) and the elongation at break were computed directly from the strength *vs* elongation curves with the help of the "Texture Exponent 32" software. Young's modulus was calculated as the slope of the initial linear portion of this curve.

2.4.4. Water-soluble fraction

The film water-soluble fraction (S) was determined by employing the methodology described by Gontard, Guilbert, and Cuq (1992). Three discs (diameter: 20 mm) of each film were cut and stored in a desiccator containing silica gel (~0% RH) for 48 h. The film samples were weighed, to obtain the initial dry weight, and immersed into 50 mL of water containing sodium azide (0.2 g/L) at 25 °C for 24 h, under sporadic agitation. The solution containing the samples was filtered, and insoluble matter was dried at 105 °C for 24 h. The resulting material was weighed for final dry weight determination. Analyses were carried out in quadruplicate, and the film water-soluble fraction (*S*, %) was calculated according to Eq. (2).

$$S = \frac{(W_i - W_f)}{W_i} x\ 100 \quad (2)$$

where W_i is the initial dry weight of the sample (g), and W_f is the final dry weight of the sample (g).

2.4.5. Water vapor permeability (WVP)

WVP was determined by standard gravimetric method E96-00 (ASTM, 2000) with some modifications. The film samples (diameter: 0.06 m) was placed on the circular opening (area: 0.00196 m^2) of a permeation cell and was sealed with sealant ring, to ensure that humidity migration would occur only through the film. The interior of the cell was filled with saturated $MgCl_2$ saline solution (33% RH) and the system was stored in a desiccator containing saturated $NaNO_2$ solution (64% RH) at 25 °C. The weight gain was monitored every 30 min, for 8 h. The analyses were conducted in triplicate. WVP was calculated using Eq. (3) and expressed in g/(ms Pa).

$$WVP = \frac{w}{t} \cdot \frac{\delta}{A.\ \Delta P} \quad (3)$$

where: w/t is the slope of the line of weight gain (w) as a function of time (t) (g/s); δ is the mean sample thickness (m); A is the sample permeation area (m^2); and ΔP is the difference in water vapor pressure through the sample for pure water at 25 °C (Pa).

2.4.6. Water uptake (WU)

The water absorption kinetics was determined according to the method described by Dufresne, Dupeyre, and Vignon (2000). Films with 20 × 20 mm dimension, with known thickness, were stored in a desiccator containing silica gel (~0% RH) for 48 h. After this period, the films were weighted and conditioned at 25 °C in hermetically sealed flasks containing Na_2SO_4 saturated solution (RH: 95%). The samples were removed at desired time intervals and weighted until equilibrium state was reached. *WU* was calculated by means of Eq. (4).

$$WU = \frac{W_t - W_0}{W_0} x\ 100 \quad (4)$$

where: *WU* is the water uptake (%), W_t is the sample weight (g) after exposure to 95% RH at time *t*, and W_0 is the initial sample weight (g).

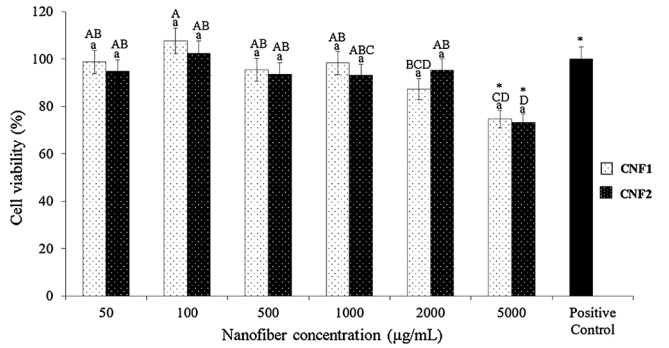

Fig. 1. CNF (CNF1 and CNF2) effect on Caco-2 cell viability after 24 h of incubation (bars represent standard deviation).
[a] Same lowercase letter superscripts in the same concentration indicate no statistically significant difference between samples ($p \geq 0.05$). [ABCD] Different uppercase letter superscripts indicate statistically significant difference between the samples in the different concentrations ($p \leq 0.05$). * Asterisks denote a significant difference relative to the positive control group ($p \leq 0.05$).

2.4.7. Optical properties and light transmittance

The color and opacity analysis of the films were performed using a colorimeter (UltraScan VIS, HunterLab, Virginia, EUA) operating in the transmittance mode, with classification system CIELab and illuminant D65 (daylight) (Hunterlab, 1996). The color parameters were directly classified by EasyMatch QC software: L (white: 100, black: 0); a (red: positive, green: negative); b (yellow: positive; blue: negative); and haze (opacity). The color difference (ΔE*) was determined using Eq. (5):

$$\Delta E^* = [(a^* - a_0^*)^2 + (b^* - b_0^*)^2 + (L^* - L_0^*)^2]^{1/2} \quad (5)$$

where: L^*: is the sample degree of lightness; L_o^*: is the standard degree of lightness; a^* and b^* are the sample chroma parameters; and a_o^* e b_o^* are the standard chroma parameters. The instrument was calibrated against a standard white reference plate. To calculate ΔE^*, a polyethylene film was used as standard ($L_o^* = 96.33$, $a_o^* = 0.06$ and $b_o^* = 0.28$). All the experiments were performed at least in triplicate and the results were presented as mean values.

Film light transmittance was measured by transmittance (%) using an UV visible spectrophotometer (Varian Model Gary 1 G, Mulgrave, Australia) operating in the wavelength range of 200–800 nm, with an accuracy of 0.1 nm. At least, three replicates of each sample were tested.

2.4.8. Fourier-transform infrared spectroscopy (FTIR)

The functional groups of the film samples were analyzed by FTIR. The film samples were cut into small pieces (10 × 10 mm) and dehydrated in a desiccator containing silica gel (~0% RH) for 3 weeks. The FTIR spectra were recorded on a spectrophotometer (PerkinElmer, model Spectrum One, Ohio, USA) fitted with a Universal Attenuated Total Reflectance (UATR) device. Analysis was accomplished in the infrared region, with 16 scans, covering wavenumbers ranging from 4000 to 650 cm^{-1}, with a spectral resolution of 4 cm^{-1} (Vicentini, Dupuy, Leitzelman, Cereda, & Sobral, 2005).

2.4.9. Atomic force microscopy-based infrared spectroscopy (AFM-IR)

AFM-IR technique can characterize and identify chemical composition of samples over the diffraction limit. The FFS was poured (0.2 µL) onto a silicon substrate coated with gold. Then, the films were dried in a chamber with air circulation under controlled temperature (54 °C) and RH (48%) for a few minutes. The analysis was performed using an atomic force microscopy model nanoIR2-s from Anasys instruments (Santa Barbara, USA) and the RH was kept around 2% during the analysis.

For spectra measurements, the AFM tip is placed at a specific region and a quantum cascade laser scan from 1530 to 1845 cm^{-1} with a 1 cm^{-1} resolution. Independent from the complex optical properties of the tip, sample absorption spectrum is directly measured by analyzing the tip deflection. Also, chemical maps were acquired using the sharped AFM tip in contact mode and the pulsed quantum cascade laser adjusted at a specific wavenumber within 1530–1845 cm^{-1} range. Thermal expansion, modulated by the pulsed laser occured when the chemical bonds was excited. Then, an AFM tip scanned the sample surface to acquire topographical information, as well as chemical maps by monitoring the cantilever deflection at the IR source frequency.

2.5. Statistical analyses

One-way analysis of variance (ANOVA) and a Tukey test of multiple comparisons with a significance level of 5% ($p \leq 0.05$) were run using Statistica software (StatSoft Inc, Tulsa, Oklahoma, USA).

3. Results and discussion

3.1. CNF effect on cell viability

The rapid dissemination of nanomaterial for commercial applications can bring a negative impact to human health. Nanoparticles can cause cytotoxicity because of their nanometer size, shape, chemical or physical properties and high reactivity (Xu et al., 2014). In order to evaluate any potential CNF cytotoxicity, Caco-2 cells were exposed to different CNFs concentrations for 24 h. The CNF1 and CNF2 (obtained by enzymatic hydrolysis) effect on Caco-2 cell viability is shown in Fig. 1.

It was observed that the CNF concentration is dependent on the activity after exposure. In general, Caco-2 cells viability slightly decreased as the concentration of CNFs increased (Fig. 1). Comparing to the positive control group (i.e., 100% cell viability), the cell viability was not significantly affected ($p \geq 0.05$) after exposure to 50, 100, 500, 1000 and 2000 µg/mL CNFs. However, cells exposed to CNF1 and CNF2 samples at 5000 µg/mL significantly reduced ($p \leq 0.05$) cell viability to 74.59% and 73.13%, respectively, when compared to the positive control group. These values were much higher than those observed by Pereira et al. (2013). These authors produced cotton CNFs with similar needle-like shape and found that cotton CNFs concentrations higher than 2000 µg/mL were toxic to fibroblast cells cultured *in vitro*. Besides, high CNFs concentration caused a sharp decrease on cell viability and affected the expression of stress and apoptosis associated to molecular markers. In another study, Alexandrescu et al. (2013) performed cytotoxicity tests demonstrating that the neat cellulose nanofibrils, from *Eucalyptus* and *Pinus radiata* pulp fibers, do not exert acute toxic phenomena on the tested fibroblast cells (3T3 cells).

Moreover, ζ-potential, which indicates the stability or aggregation tendency in the dispersion, is a critical parameter. In our study, CNF1 and CNF2 samples showed high negative ζ-potential values of −29.1 and −31.5 mV, respectively (Table 1), which promoted stable colloidal suspensions that prevented CNFs aggregation. Consequently, no negative effect on cell viability was observed, since agglomerated nanofibers could promote a cell cytotoxicity induction (Pereira et al., 2013). Even though earlier studies reported CNF low or non-toxic effect, the issues related to safety of these natural nanomaterial should be further assessed when used as food packaging. Once incorporated in biodegradable films, CNFs will presumably be unable to migrate out of the films' structure, thus posing virtually no danger to the consumers or the environment. In any case, final material safety evaluation (*e.g.*, regarding CNFs migration) need to be performed in future works. However, our study showed that a CNFs maximum amount of 2000 µg/mL can be used without compromising cell viability.

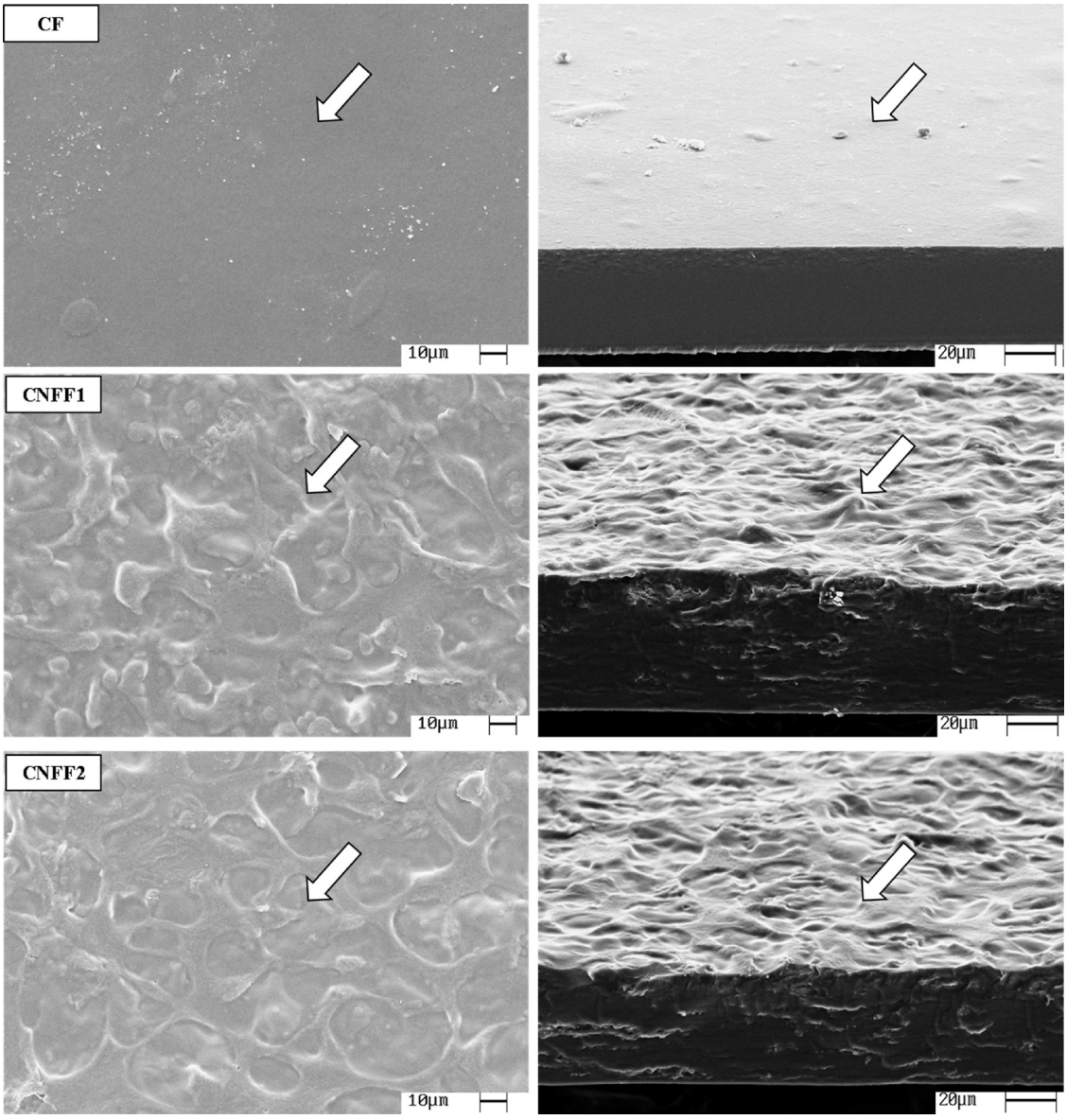

Fig. 2. SEM images of surface (1000×, scale bar = 10 μm) and cross-section (1000×, scale bar = 20 μm) of the control film (CF) and nanocomposite films reinforced with cellulose nanofibers (CNFF1 and CNFF2).

3.2. Nanocomposite films characterization

3.2.1. Topography and roughness

The surface and cross-section of the nanocomposite films were analyzed by SEM for microstructure evaluation (Fig. 2). The CNFs incorporation significantly changed the CNFF1 and CNFF2 films' microstructure as compared with CF. The CF film displayed a more uniform and smoother surface (see arrows in Fig. 2; CF) while, nanocomposite films presented non-homogenous structures, i.e., irregular surface (see arrows in Fig. 2; CNFF1 and CNFF2). In addition, the cross-section SEM images showed that nanocomposite films exhibited less dense and less homogeneous polymeric structure with small cracks, as compared with the control film. Each CNF fraction had a different aspect ratio, surface charge and crystallinity (Table 1). Thus, these characteristics can contribute for the type of interactions between cellulose and polymer matrix components resulting in distinct microstructures. Moreover, the presence of other components (starch, water and glycerol) in the film formulation may had contributed to the slightly less organized structures which consisted of multilayers compacted along the nanocomposite film cross-section (Pelissari et al., 2017).

Fig. 3 shows the AFM images of the CF, CNFF1 and CNFF2 sample films obtained from AFM topography, amplitude and phase signals. The roughness value of CF was 4.10 nm, which increased to 16.58 nm (CNFF1) and 11.6 nm (CNFF2) when CNFs were incorporated into the starch matrix. Considering that CNF1 are shorter (length and diameter) than CNF2, the higher CNFs number per unit area in the films can explain the rougher film structure. Similar results for nanocomposite films reinforced with CNFs (successively passed through high-pressure homogenizer) were reported by Moura et al. (2011) and Pelissari et al. (2017).

The rougher CNFF1 film structure could be also due to the higher CNF1 aggregation in the starch matrix. CNF2 presented a slightly higher and negative ζ-potential value (i.e., −31.5 mV) (Table 1), conferring good CNFs stability. Besides, CNF1 showed lower crystallinity index (61.5%) than CNF2 (66.2%) which implies that CNFF1 had amorphous compounds fractions (*e.g.*, lignin and hemicellulose) that contributed to the increased of film roughness.

CNFF1 showed a more uniform surface and smooth than CNFF2. This could be due to the more homogeneous nanofiber distribution into the starch matrix caused by CNF1 high aspect ratio value (i.e., 404.5).

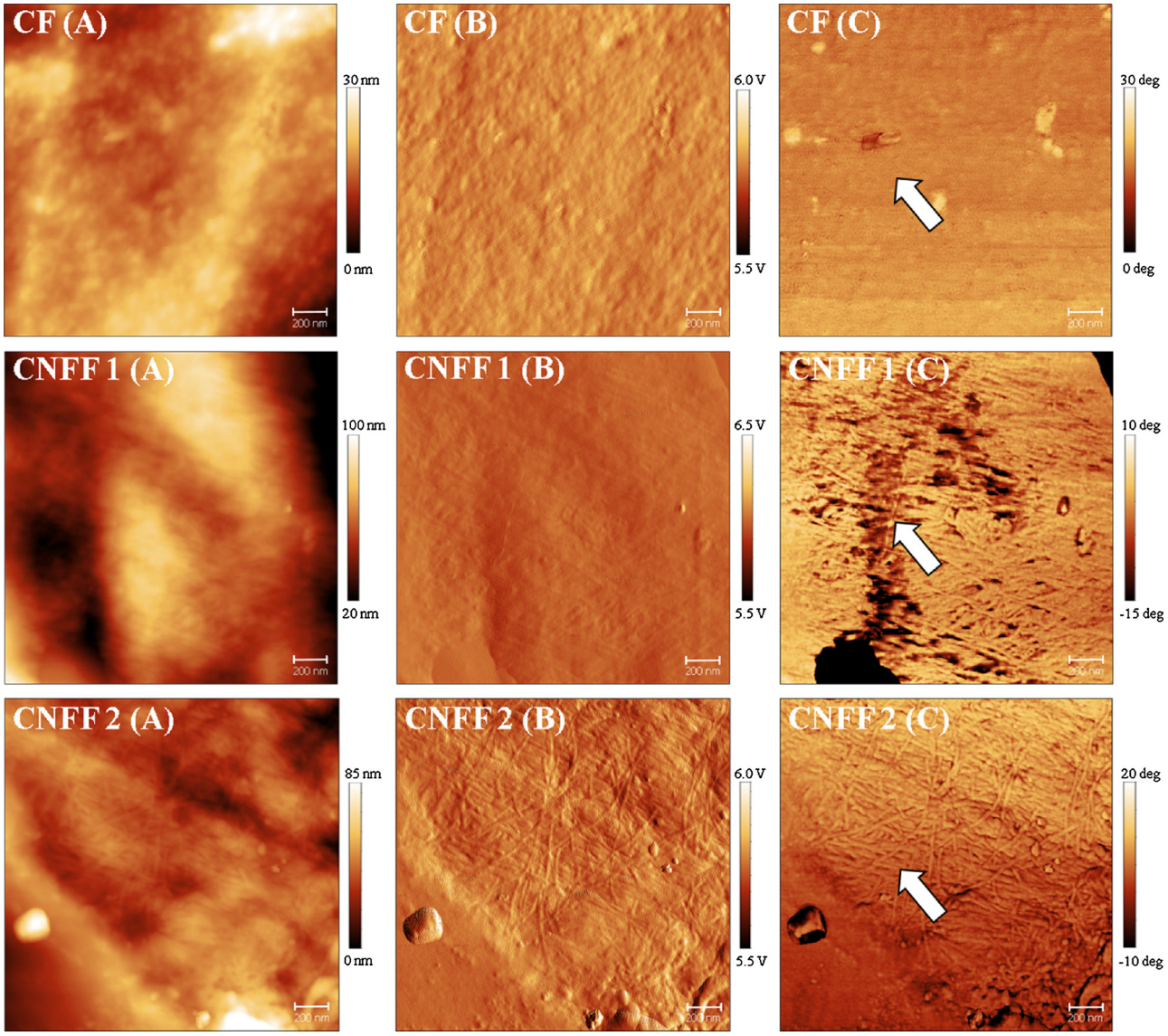

Fig. 3. AFM images of the nanocomposite films: CF, CNFF1 and CNFF2 obtained from topography signal (A), amplitude (B) and phase (C) images (scanning area: 2.0 × 2.0 µm, scale bar: 200 nm).

Table 2
Thickness, density, mechanical properties and water barrier properties of the control film (CF) and nanocomposite films reinforced with cellulose nanofibers (CNFF1 and CNFF2).

Film	Thickness (µm)	Density (g/cm^3)	Tensile strength (MPa)	Elongation at break (%)	Young's modulus (MPa)	Moisture (%)	Solubility in water (%)	WVP (10^{-11} g/ms Pa)
CF	76 ± 0.2^a	1.40 ± 0.02^b	8.9 ± 0.1^a	83.2 ± 0.7^b	288.8 ± 0.01^a	18.61 ± 0.03^b	32.3 ± 0.16^c	11.5 ± 1.1^b
CNFF1	78 ± 0.8^a	1.27 ± 0.02^a	96.6 ± 2.1^c	50.0 ± 8.0^a	2064.1 ± 476.2^b	13.41 ± 1.49^a	20.9 ± 0.00^a	6.4 ± 0.4^a
CNFF2	76 ± 0.8^a	1.27 ± 0.04^a	65.5 ± 3.4^b	52.1 ± 8.6^a	805.3 ± 77.5^a	12.80 ± 0.10^a	27.9 ± 0.05^b	16.6 ± 0.5^c

^{a,b,c} Different letter superscripts in the same column indicate a statistically significant difference ($p \leq 0.05$).

Despite the different film microstructures, starch matrix coated CNFs on both nanocomposite films, implying that CNFs showed good adhesion to the biopolymer matrix.

3.2.2. Thickness and density

Table 2 shows the results of thickness and density of the produced films. During the casting procedure, the FFS was employed for strict control of the dry mass content per unit area of plate. This approach helped to achieve similar film thickness values ($p \geq 0.05$). The incorporation of CNFs in nanocomposite films reduced significantly the density ($p \leq 0.05$) in comparison to CF, as a result of the CF microstructure. SEM cross-section micrographs (Fig. 2) showed that the nanocomposite structure is more open, more porous, and less dense than the CF structure.

3.2.3. Mechanical properties

Results of the film mechanical properties (tensile strength, elongation at break and Young's modulus) are presented in Table 2. The nanocomposite films presented lower elongation at break values, and higher values of tensile strength ($p \leq 0.05$) and Young's modulus than

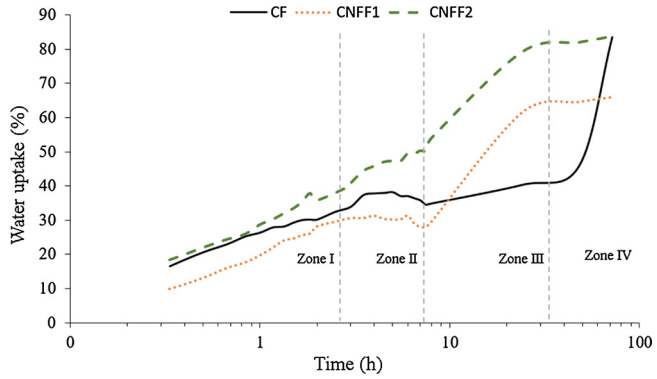

Fig. 4. Water uptake (%) during conditioning at 95% RH as a function of time for the control film (CF) and nanocomposite films reinforced with cellulose nanofibers (CNFF1 and CNFF2).

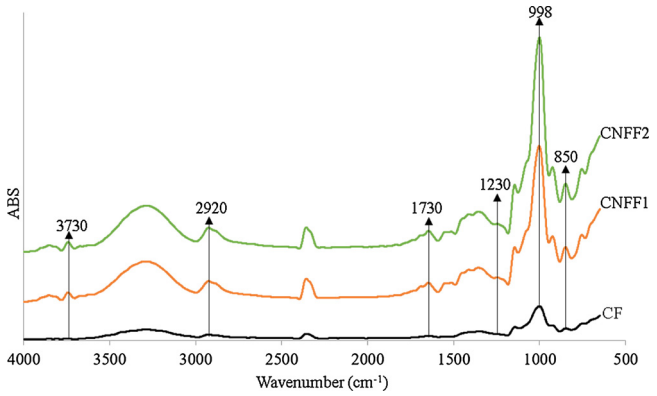

Fig. 5. FTIR spectra of the control film (CF) and nanocomposite films reinforced with cellulose nanofibers (CNFF1 and CNFF2), cellulose nanofiber suspension and pure banana starch.

CF. Young's modulus was the most affected by CNFs, since this parameter increased more than 100% with CNFs addition. CNFs incorporation into the starch matrix resulted in strong interactions between cellulose crystallites and starch, which restricted the starch matrix chain motion (Lu, Weng, & Cao, 2005).

The nanofiber's aspect ratio might be a parameter exerting influence on the films' mechanical properties (Iwamoto, Nakagaito, & Yano, 2007). The nanocomposite films reinforced with CNF1 (i.e., higher aspect ratio: 404.5) were more rigid and brittle than the films reinforced with CNF2 (i.e., lower aspect ratio: 170.2). Considering that CNF1 showed lower length and diameter (Table 1) than CNF2, the CNFs number per unit area in the films could explain a formation of a more homogeneous, interconnected and rigid structure with a reduction of CNFF1 film elongation. Therefore, the films' mechanical properties seem to be affected by the CNF size.

3.2.4. Water barrier properties

Nanocomposite films reinforced with CNFs showed significant lower moisture values ($p \leq 0.05$) compared to CF (Table 2). CF presented higher solubility than the other films due to the highly hydrophilic nature of the starch-based films (Table 2). The nanocomposite films were less water-soluble (i.e., 14–36% reduction) compared to the CF ($p \leq 0.05$), indicating that the starch film water affinity was significantly affected by the CNFs incorporation. Comparing both nanocomposite films, CNFF1 showed lower solubility in water than CNFF2 ($p \leq 0.05$). The presence of CNFs in starch matrix film reduced the contact of the water with hydrophilic groups, because CNFs have low affinity for water molecules (Müller, Laurindo, & Yamashita, 2009). Films slightly soluble in water are more indicated for food protection against high water activity (Gontard et al., 1992).

WVP values can be a indicator of food product type that can be packed in the film (*e.g.*, fresh or dehydrated). The films' water vapor barrier ability was tested in a specific RH gradient (33–64%) and the results are shown in Table 2. CNFF1 showed a significant decrease in WVP value when compared to the CF ($p \leq 0.05$). However, CNFF2 had the highest WVP value compared to all samples ($p \leq 0.05$). A lower WVP means that less water vapor passes through the film, which indicates stronger water vapor barrier ability. The water molecules difficulty to penetrate the cellulose crystalline region is associated to the increased material tortuosity due to nanofibers presence, and also because, proportionally, there are fewer hydrophilic sites (Pelissari et al., 2017; Lavoine, Desloges, Dufresne, & Bras, 2012; Yu et al., 2017). Thus, the nanofiber-network hinders the contact between starch hydrophilic groups and water molecules and reduces the water diffusion through the matrix (Lomelí Ramírez et al., 2011; Yu et al., 2017).

Therefore, water barrier properties values are dependent on CNF filler size and aspect ratio. As observed, CNF2 suspension had higher diameter and length size (Table 1) and consequently, lower aspect ratio than CNF1, which tend to agglomerate and facilitate the water molecules permeation through the polymer matrix gaps. Pelissari et al. (2017) also reported that the smallest nanofibers incorporated into starch matrix decreased solubility and WVP values. Smaller nanofibers are more properly dispersed and entangled inside the matrix than the longer ones.

Fig. 4 shows CF and nanocomposite films' WU results. The water diffusion kinetics was higher in the first hours of analysis. All films presented a WU increase with constant rate until 3 h of analysis (zone I), forming a plateau from 3 h to 8 h (zone II). CF water absorption kinetics was slower than the other films after 8 h of analysis, resulting in a plateau until 48 h (zone III). After 48 h, CF WU values dramatically increased until the last hours of analysis (zone IV). Conversely, nanocomposite films' WU values increased until 48 h of analysis (zone III) and thereafter, remained constant, reaching a new plateau (zone IV). CNFF1 presented lower WU in the zone I as compared with the CF and CNFF2 (CNFF1 < CF < CNFF2). Regarding the zone II, nanocomposite films showed higher WU than CF (CF < CNFF1 < CNFF2). On the other hand, WU of the nanocomposite films (zone IV) remained constant, while CF WU rapidly increased and exceeded the values obtained for nanocomposite films at 72 h of analysis.

The higher CF WU was a characteristic of the starch hygroscopic nature, which made it prone to water absorption. Nanocomposite films showed significant differences for WU kinetic parameters ($p \leq 0.05$) despite the same banana starch, CNF and glycerol content in all the composite films. CNFs with high aspect ratio added to films increased the starch-based composite films' water-resistance. The film water absorption reduction was strongly related to the diminished diffusion

Table 3
Optical properties and light transmittance of control film (FC) and nanocomposites reinforced with cellulose nanofibers (CNFF1 and CNFF2).

Film	L*	a*	b*	ΔE*	Opacity (%)	UV % (400 nm region)	UVB % (300 nm region)
CF	95.39 ± 0.05^{b}	−0.02 ± 0.01^{a}	1.04 ± 0.01^{a}	2.19 ± 0.04^{a}	29.5 ± 0.3^{a}	72 ± 0.01^{b}	68 ± 0.01^{b}
CNFF1	62.46 ± 0.13^{a}	0.38 ± 0.00^{b}	4.60 ± 0.01^{b}	31.17 ± 0.13^{b}	70.53 ± 0.05^{c}	39 ± < 0^{a}	24 ± < 0^{a}
CNFF2	62.66 ± 0.13^{a}	0.50 ± 0.01^{c}	5.20 ± 0.04^{c}	31.06 ± 0.13^{b}	69.43 ± 0.05^{b}	40 ± 0.01^{a}	26 ± 0.02^{a}

^{a,b,c} Different letter superscripts in the same column indicate a statistically significant difference ($p \leq 0.05$).

Table 4
Main bands of the FTIR spectra for control film (FC) and nanocomposite films reinforced with cellulose nanofibers (CNFF1 and CNFF2).

Sample	Band region (cm^{-1})	Assignment	Component	References
CF and nanocomposites	3270	Stretching vibrations of the hydrogen bonding −OH	Starch	Chen et al. (2009)
	2330–2350	Coupling of asymmetric NH and CH stretching vibration	Proteins attached with starch	Lian, Zhu, Wen, Li, and Zhao, (2013)
		−OH stretching	Cellulose II	Andrade-Mahecha et al. (2015)
	1642–1652	Stretching vibration of the C=O bond	Amide I – protein of starch	Ahmad et al. (2012)
		Bending vibrations of −OH	Starch	Chen et al., 2009
	1150	C−O and C−C groups	Starch	Araujo-Farro (2008) and Huang, Jeng, Sain, Saville, and Hubbes, (2006)
	920	Glycosidic bonds	Starch (amylopectin α-1,6 bonds)	Kizil, Irudayaraj, and Seetharaman, (2002)
	850	Stretching of C−O−C and CH and CH_2 deformation	Starch	Chen et al. (2009) and Pelissari et al. (2017)
	745	Aromatic structures	Phenolic compounds in starch and remaining amorphous compounds of CNFs	Pelissari, Andrade-Mahecha, Sobral, and Menegalli, (2013)
CF	1460–1260		Amide III – protein of starch	Pelissari et al. (2013)
	990	Stretching vibration of C−O	Starch	Chen, Cao, Chang, and Huneault, (2008) and Van Soest, Hulleman, de Wit, and Vliegenthart, (1996)
Nanocomposites	3730	−OH groups	Water absorbtion by starch	Kaushik, Singh, and Verma, (2010)
	2920	Aliphatic saturated C−H stretching vibration	Cellulose and hemicellulose	Cherian et al. (2008)
	1730	Acetyl and uronic ester groups vibration	Lignin and hemicellulose	Alemdar and Sain (2008), Cherian et al. (2008) and Sun, Xu, Sun, Xiao, and Sun, (2005)
	1336	Bending of −COH and −CH groups	Cellulose	Pelissari et al. (2017)
	1230	Stretching vibrations of C−O	Cellulose and residual lignin and hemicellulose	Cherian et al. (2008)
	998	C−O and C−H vibration	Cellulose	Sun et al. (2005)

coefficient imposed by the nanofibers (Pelissari et al., 2017). This means that the starch-based film with fiber at nanoscale had higher water-resistance than the original starch-based film.

3.2.5. Optical properties and light transmittance

Optical properties are important features for film applications, particularly if the film is used as food surface coating or food packaging. All optical properties results' showed statistically significant differences ($p \leq 0.05$) between CF and nanocomposite films (Table 3). Compared with CF, film luminosity (L*) decreased and opacity increased, upon addition of CNFs. Thus, their incorporation into the starch matrix produced darker and less translucent films (L*, CF > nanocomposite) than the CF.

Nanocomposite films a* and b* values significantly increased ($p \leq 0.05$), indicating that films with CNFs were more yellowish and reddish compared to CF. Therefore, ΔE* of nanocomposite films increased because a* and b* values increased and L* values decreased ($p \leq 0.05$). Based on the L*, a*, b*, and ΔE* values, addition of CNFs prompted a great matrix disorder in the banana starch film which, may had contributed to the changes occurred in films' optical properties. Furthermore, CF was more transparent than the nanocomposite films (Table 3), implying that CNFs film reinforcement increased 135–138% opacity. This phenomenon may be occurred due the CNF nanometer size, high aspect ratio and to strong interactions between the CNFs and starch matrix (Pelissari et al., 2017). CNFF1 showed higher opacity values compared with CNFF2 ($p \leq 0.05$), probably due to CNFs random distribution in the starch matrix, since the addition of CNFs showed a more homogeneous dispersion within the composite film diminishing even more its transparency (Bilbao-Sáinz, Avena-Bustillos, Wood, Williams, & McHugh, 2010).

The CF and nanocomposite films light transmittance results in the 200–800 nm wavelength range are shown in Table 3. Nanocomposite films presented light transmittance values significantly lower ($p \leq 0.05$) than CF at the same wavelength, indicating once more, that CNFs decreased starch film transparency. UV region corresponds to wavelengths ranging from 200 to 400 nm (Chen, Liu, Chang, Cao, & Anderson, 2009). Overall, nanocomposite films light transmittance values were lower than CF in the UV region, indicating that CNFs addition increased nanocomposite films UV light absorption.

Therefore, CNFs addition to films form an extra barrier to light transmittance in a wide wavelength range because those fibers confer high opacity and yellowness to the films (Table 3). Also, the incorporation of CNFs made films darker and a more effective barrier against UV and UVB light when compared to CF ($p \leq 0.05$). The remaining proteins from the starch isolation process might have increased the UV-barrier due the high content of aromatic amino acids (protein structure) that absorbed UV light (Ahmad, Benjakul, Prodpran, & Agustini, 2012). Thus, these results showed that nanocomposite films could be a good UV/vis light barrier to prevent lipid oxidation of food products.

3.2.6. Fourier-transform infrared spectroscopy (FTIR)

FTIR analysis was conducted to monitor the film functional groups and possible structure interactions. The IR spectra results of the CF and the nanocomposite films are shown in Fig. 5.

Moreover, the main CF and nanocomposite films' FTIR bands observed and their assignments are summarized in Table 4. Films spectra exhibited almost the same peaks due to starch and cellulose chemical similarities. FTIR results showed that the functional groups presented on cellulose and starch surface led to good physical interactions between the two molecules. Besides, the CNFs were well dispersed in the starch matrix, which improved the nanocomposite films' performance.

3.2.7. Atomic force microscopy-based infrared (AFM-IR) spectroscopy

IR spectroscopy is a powerful tool for spatial mapping chemical content in a wide variety of applications (Prater, Kjoller, & Shetty,

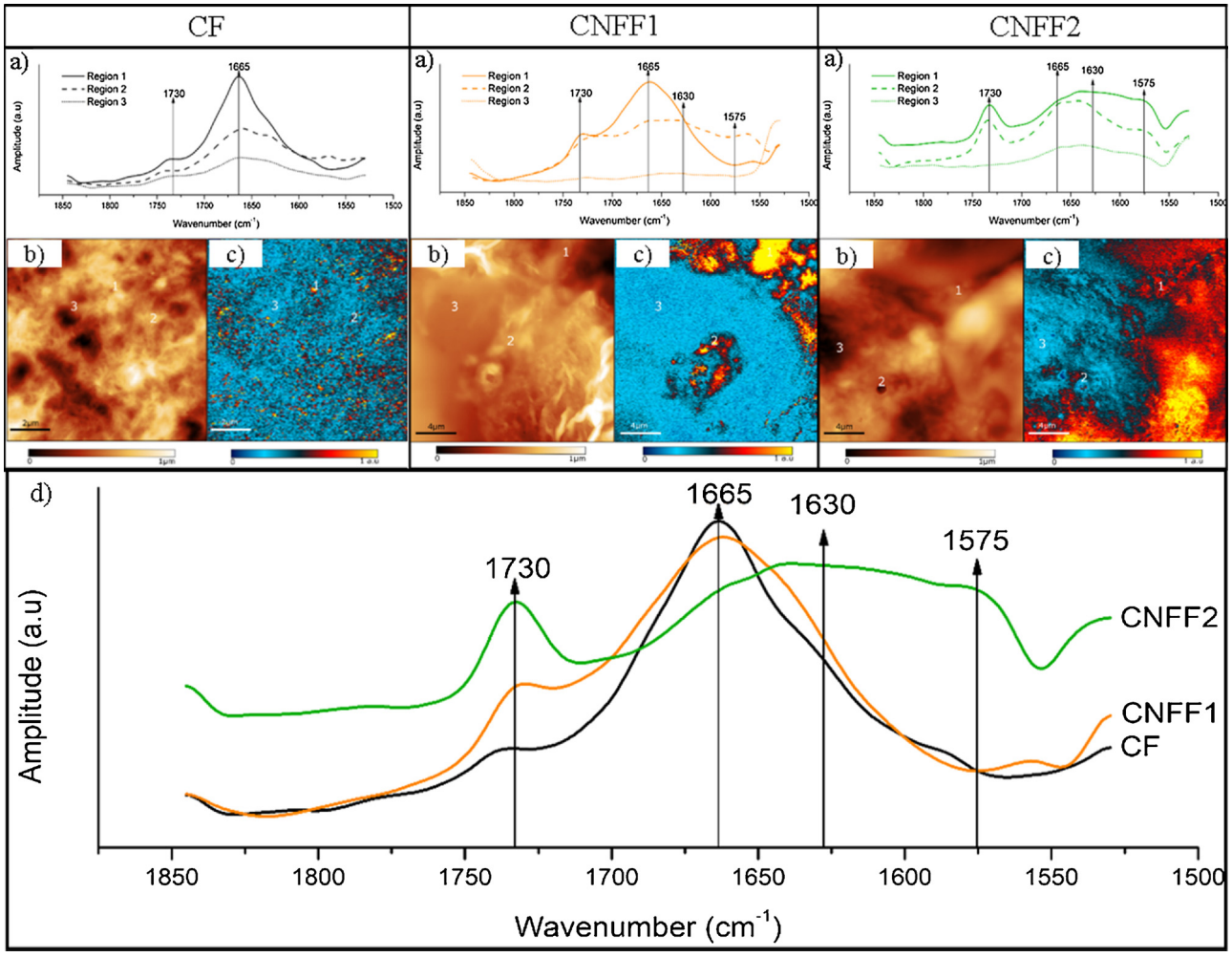

Fig. 6. AFM-IR images of control film (CF) and nanocomposite films reinforced with cellulose nanofibers (CNFF1 and CNFF2): infrared spectrum (a), topography (b), chemical maps with nanometer resolution (c) and comparison between infrared spectra of all films (d).

2010). The AFM-IR spectroscopy became a complementary FTIR technique, since topographic information is correlated with the local chemical analysis. The AFM-IR technique breaks the diffraction limits combining the precise IR spectroscopy chemical identification with the nanoscale AFM capabilities, to chemically identify sample components with spatial resolution down to 10 nm.

It was possible to acquire CF and nanocomposite films IR spectra with this technique, as well as chemical maps with nanometer resolution (Fig. 6). The films images were taken by adjusting the IR source to a fixed wavenumber (i.e., 1660 cm^{-1}).

CF IR spectrum (Fig. 6a; CF) showed two distinct peaks. An intense IR absorption band was observed at 1665 cm^{-1} region originated from amide I (protein amide group bounded to starch). The minor bands between 1740 and 1730 cm^{-1} in the pure starch IR spectra were attributed to the C═O (Nobrega, Olivato, Müller, & Yamashita, 2012). The CF chemical map image (Fig. 6c; CF) was homogeneous with similar chemical component distribution at the nanoscale without contrasts as confirmed by the clear color blue predominance.

The CNFF1 IR spectra (Fig. 6a; CNFF) showed a peak at 1665 cm^{-1} and a shoulder at 1730 cm^{-1} in the region 1 which corroborated the FTIR results (Fig. 5b). Regarding region 2, it was possible to observe a peak at 1630 cm^{-1} suggesting that new hydrogen bonding interactions between cellulose and starch molecules were formed as a result of CNFs addition to starch (Chen et al., 2009). This peak can be attributed to the bending vibrations of the hydrogen bonding −OH groups of cellulose and, may also be attributed to the C═C vibration, an indication of the lignin presence (Cherian et al., 2008). Also, it was possible to found in the regions 1 and 2, a peak around 1575 cm^{-1} attributed to amide II. The region 3 showed a uniform absorption because in this region only gold substrate was measured. The AFM-IR images acquired at 1660 cm^{-1} showed that the functional group of the amide I tended to agglomerate in the CNFF1 and CNFF2 films. Such agglomeration can only be observed due to the high resolution of the AFM-IR technique for chemical imaging.

IR spectra of the all produced films are presented in Fig. 6d. The peak at 1730 cm^{-1} was more pronounced in films with CNFs incorporated (being more intense on CNFF2) than in CF. This result may be associated with the higher amount of aromatic groups present in CNF1 than CNF2 samples. All samples showed similarity in the peak at 1665 cm^{-1} which was related to starch. The peaks at 1630 and 1575 cm^{-1} were more pronounced in CNFF2 sample, which may be related with the CNF2 higher aspect ratio, enhancing starch and CNF interactions.

4. Conclusion

CNFs produced from unripe banana peel by enzymatic hydrolysis were potentially applicable as a reinforcing agent in composite films. Produced CNFs did not show toxicity effect on the Caco-2 cells for studied concentrations lower than 1000 mg/mL. However, toxicity assessment as well as evaluation of possible CNFs characteristic modification during production process is required for human and

environment safety, before these materials could be considered safe for potential food applications.

The film used as food packaging must avoid or at least decrease moisture transfer between food and the surrounding atmosphere. The addition of CNFs into starch matrix proved to be an effective approach to increase water barrier and mechanical-resistance of banana starch films. Furthermore, the nanocomposites displayed high opacity and low luminosity, which translated into reduced UV and UVB transmittance values. CNFF1 film showed more advantageous properties (*e.g.*, lower WVP and water solubility) compared to CF and CNFF2 films. This can be attributed to employed CNFs lower size and higher aspect ratio which that led to a more suitable dispersion and entanglement in the starch film matrix.

Therefore, unripe banana peel is a potential starch and CNFs source that can be applied as matrix and reinforcing material in biodegradable films, respectively. These compounds are biocompatible and biodegradable, which enables their use in the food packaging industry.

Acknowledgments

The authors would like to acknowledge the financial support provided by Conselho Nacional de Desenvolvimento Científico e Tecnológico (CNPq) (140274/2014-6), Coordenação de Aperfeiçoamento de Pessoal de Nível Superior (CAPES) (2952/2011) and CAPES/FCT número349/13 for Ph.D internship program. Joana T. Martins acknowledges the Foundation for Science and Technology (FCT) for her fellowship (SFRH/BPD/89992/2012). This study was supported by FCT under the scope of the strategic funding of UID/BIO/04469/2013 unit and COMPETE 2020 (POCI-01-0145-FEDER-006684) and BioTecNorte operation (NORTE-01-0145-FEDER-000004) funded by the European Regional Development Fund under the scope of Norte2020 - Programa Operacional Regional do Norte. The authors would also like to acknowledge the Brazilian Nanotechnology National Laboratory (LNNano) for allocation of the TEM, AFM and AFM-Nano IR apparatus.

References

Ahmad, M., Benjakul, S., Prodpran, T., & Agustini, T. W. (2012). Physico-mechanical and antimicrobial properties of gelatin film from the skin of unicorn leatherjacket incorporated with essential oils. *Food Hydrocolloids, 28*(1), 189–199.

Alemdar, A., & Sain, M. (2008). Biocomposites from wheat straw nanofibers: Morphology, thermal and mechanical properties. *Composites Science and Technology, 68*(2), 557–565.

Alexandrescu, L., Syverud, K., Gatti, A., & Chinga-Carrasco, G. (2013). Cytotoxicity tests of cellulose nanofibril-based structures. *Cellulose, 20*(4), 1765–1775.

Andrade-Mahecha, M. M., Pelissari, F. M., Tapia-Blácido, D. R., & Menegalli, F. C. (2015). Achira as a source of biodegradable materials: Isolation and characterization of nanofibers. *Carbohydrate Polymers, 123*, 406–415.

Antunes, F., Andrade, F., Araujo, F., Ferreira, D., & Sarmento, B. (2013). Establishment of a triple co-culture in vitro cell models to study intestinal absorption of peptide drugs. *European Journal of Pharmaceutics and Biopharmaceutics, 83*(3), 427–435.

AOAC (2005). *Official methods of analysis* (18 th ed.). Washington: Association of Official Analytical Chemists.

Araujo-Farro, P. C. (2008). *Development and optimization of biodegradables films made of products derivated from "royal" variety quinoa (Chenopodium quinoa Willdenow) seeds.* PhD thesis, Unicamp, Brazil.

ASTM (2000). *Standard test method of water vapor transmission of materials (E96-00). Annual book of ASTM standards.* Philadelphia: American Society for Testing and Materials.

ASTM (2012). *Standard test method for tensile properties of thin plastic sheeting (D882-12). Annual book of ASTM standards.* Philadelphia: American Society for Testing and Materials.

Bilbao-Sáinz, C., Avena-Bustillos, R. J., Wood, D. F., Williams, T. G., & McHugh, T. H. (2010). Composite edible films based on hydroxypropyl methylcellulose reinforced with microcrystalline cellulose nanoparticles. *Journal of Agricultural and Food Chemistry, 58*(6), 3753–3760.

Chen, Y., Cao, X., Chang, P. R., & Huneault, M. A. (2008). Comparative study on the films of poly(vinyl alcohol)/pea starch nanocrystals and poly(vinyl alcohol)/native pea starch. *Carbohydrate Polymers, 73*(1), 8–17.

Chen, Y., Liu, C., Chang, P. R., Cao, X., & Anderson, D. P. (2009). Bionanocomposites based on pea starch and cellulose nanowhiskers hydrolyzed from pea hull fibre: Effect of hydrolysis time. *Carbohydrate Polymers, 76*(4), 607–615.

Cherian, B. M., Pothan, L. A., Nguyen-Chung, T., Mennig, G., Kottaisamy, M., & Thomas, S. (2008). A novel method for the synthesis of cellulose nanofibril whiskers from banana fibers and characterization. *Journal of Agricultural and Food Chemistry, 56*(14), 5617–5627.

Clift, M. J. D., Foster, E. J., Vanhecke, D., Studer, D., Wick, P., Gehr, P., et al. (2011). Investigating the interaction of cellulose nanofibers derived from cotton with a sophisticated 3D human lung cell coculture. *Biomacromolecules, 12*(10), 3666–3673.

Dufresne, A., Dupeyre, D., & Vignon, M. R. (2000). Cellulose microfibrils from potato tuber cells: Processing and characterization of starch-cellulose microfibril composites. *Journal of Applied Polymer Science, 76*(14), 2080–2092.

Elanthikkal, S., Gopalakrishnapanicker, U., Varghese, S., & Guthrie, J. T. (2010). Cellulose microfibres produced from banana plant wastes: Isolation and characterization. *Carbohydrate Polymers, 80*(3), 852–859.

Gómez, C., Zuluaga, R., Putaux, J.-L., Mondragon, I., Castro, C., & Gañán, P. (2012). Surface free energy of films of alkali-treated cellulose microfibrils from banana rachis. *Composite Interfaces, 19*(1), 29–37.

Gontard, N., Guilbert, S., & Cuq, J.-L. (1992). Edible wheat gluten films: Influence of the main process variables on film properties using response surface methodology. *Journal of Food Science, 57*(1), 190–195.

Huang, C. B., Jeng, R., Sain, M., Saville, B. A., & Hubbes, M. (2006). Production, characterization and mechanical properties of starch modified by Ophiostoma spp. *Bioresources, 1*(2), 257–269.

Hunterlab (1996). *Application note: CIE L* a* b* color scale, Vol. 8* Virginia.

Iwamoto, S., Nakagaito, A. N., & Yano, H. (2007). Nano-fibrillation of pulp fibers for the processing of transparent nanocomposites. *Applied Physics A, 89*(2), 461–466.

Jones, C. F., & Grainger, D. W. (2009). In vitro assessments of nanomaterial toxicity. *Advanced Drug Delivery Reviews, 61*(6), 438–456.

Kaushik, A., Singh, M., & Verma, G. (2010). Green nanocomposites based on thermoplastic starch and steam exploded cellulose nanofibrils from wheat straw. *Carbohydrate Polymers, 82*(2), 337–345.

Kizil, R., Irudayaraj, J., & Seetharaman, K. (2002). Characterization of irradiated starches by using FT-Raman and FTIR spectroscopy. *Journal of Agricultural and Food Chemistry, 50*(14), 3912–3918.

Lavoine, N., Desloges, I., Dufresne, A., & Bras, J. (2012). Microfibrillated cellulose–its barrier properties and applications in cellulosic materials: A review. *Carbohydrate Polymers, 90*(2), 735–764.

Lian, X., Zhu, W., Wen, Y., Li, L., & Zhao, X. (2013). Effects of soy protein hydrolysates on maize starch retrogradation studied by IR spectra and ESI-MS analysis. *International Journal of Biological Macromolecules, 59*, 143–150.

Lima, R., Oliveira Feitosa, L., Rodrigues Maruyama, C., Abreu Barga, M., Yamawaki, P. C., Vieira, I. J., et al. (2012). Evaluation of the genotoxicity of cellulose nanofibers. *International Journal of Nanomedicine, 7*, 3555–3565.

Lomelí Ramírez, M. G., Satyanarayana, K. G., Iwakiri, S., de Muniz, G. B., Tanobe, V., & Flores-Sahagun, T. S. (2011). Study of the properties of biocomposites. Part I. Cassava starch-green coir fibers from Brazil. *Carbohydrate Polymers, 86*(4), 1712–1722.

Lu, Y., Weng, L., & Cao, X. (2005). Biocomposites of plasticized starch reinforced with cellulose crystallites from cottonseed linter. *Macromolecular Bioscience, 5*(11), 1101–1107.

Moreira, M. R. (2009). *Natureza das Interações Celulose-Água.* DissertaçãoSão Carlos: Universidade de São Paulo.

Moura, M. R., Avena-Bustillos, R. J., McHugh, T. H., Wood, D. F., Otoni, C. G., & Mattoso, L. H. C. (2011). Miniaturization of cellulose fibers and effect of addition on the mechanical and barrier properties of hydroxypropyl methylcellulose films. *Journal of Food Engineering, 104*(1), 154–160.

Müller, C. M. O., Laurindo, J. B., & Yamashita, F. (2009). Effect of cellulose fibers addition on the mechanical properties and water vapor barrier of starch-based films. *Food Hydrocolloids, 23*(5), 1328–1333.

Nobrega, M. M., Olivato, J. B., Müller, C. M. O., & Yamashita, F. (2012). Biodegradable starch-based films containing saturated fatty acids: Thermal, infrared and raman spectroscopic characterization. *Polímeros, 22*, 467–474.

Padam, B. S., Tin, H. S., Chye, F. Y., & Abdullah, M. I. (2014). Banana by-products: An under-utilized renewable food biomass with great potential. *Journal of Food Science and Technology, 51*(12), 3527–3545.

Pelissari, F. M., Andrade-Mahecha, M. M., Sobral, P. J. A., & Menegalli, F. C. (2012). Isolation and characterization of the flour and starch of plantain bananas (Musa paradisiaca). *Stärke, 64*(5), 382–391.

Pelissari, F. M., Andrade-Mahecha, M. M., Sobral, P. J. A., & Menegalli, F. C. (2013). Comparative study on the properties of flour and starch films of plantain bananas (Musa paradisiaca). *Food Hydrocolloids, 30*(2), 681–690.

Pelissari, F. M., Andrade-Mahecha, M. M., Sobral, P. J. A., & Menegalli, F. C. (2017). Nanocomposites based on banana starch reinforced with cellulose nanofibers isolated from banana peels. *Journal of Colloid and Interface Science, 505*, 154–167.

Pereira, M. M., Raposo, N. R., Brayner, R., Teixeira, E. M., Oliveira, V., Quintao, C. C., et al. (2013). Cytotoxicity and expression of genes involved in the cellular stress response and apoptosis in mammalian fibroblast exposed to cotton cellulose nanofibers. *Nanotechnology, 24*(7), 075103.

Prater, C., Kjoller, K., & Shetty, R. (2010). Nanoscale infrared spectroscopy. *Materials Today, 13*(11), 56–60.

Sun, J. X., Xu, F., Sun, X. F., Xiao, B., & Sun, R. C. (2005). Physico-chemical and thermal characterization of cellulose from barley straw. *Polymer Degradation and Stability, 88*(3), 521–531.

Tibolla, H., Pelissari, F. M., Rodrigues, M. I., & Menegalli, F. C. (2017). Cellulose nanofibers produced from banana peel by enzymatic treatment: Study of process conditions. *Industrial Crops and Products, 95*, 664–674.

Van Soest, J. J. G., Hulleman, S. H. D., de Wit, D., & Vliegenthart, J. F. G. (1996). Changes in the mechanical properties of thermoplastic potato starch in relation with changes in B-type crystallinity. *Carbohydrate Polymers, 29*(3), 225–232.

Vicentini, N. M., Dupuy, N., Leitzelman, M., Cereda, M. P., & Sobral, P. J. A. (2005). Prediction of cassava starch edible film properties by chemometric analysis of infrared spectra. *Spectroscopy Letters, 38*(6), 749–767.
Xu, X., Wang, H., Jiang, L., Wang, X., Payne, S. A., Zhu, J. Y., et al. (2014). Comparison between cellulose nanocrystal and cellulose nanofibril reinforced poly(ethylene oxide) nanofibers and their novel Shish-Kebab-like crystalline structures. *Macromolecules, 47*(10), 3409–3416.
Yu, Z., Alsammarraie, F. K., Nayigiziki, F. X., Wang, W., Vardhanabhuti, B., Mustapha, A., et al. (2017). Effect and mechanism of cellulose nanofibrils on the active functions of biopolymer-based nanocomposite films. *Food Research International, 99*(Part 1), 166–172.
Zuluaga, R., Putaux, J.-L., Restrepo, A., Mondragon, I., & Gañán, P. (2007). Cellulose microfibrils from banana farming residues: Isolation and characterization. *Cellulose, 14*(6), 585–592.

Further Reading

Guimarães, J. L., Wypych, F., Saul, C. K., Ramos, L. P., & Satyanarayana, K. G. (2010). Studies of the processing and characterization of corn starch and its composites with banana and sugarcane fibers from Brazil. *Carbohydrate Polymers, 80*(1), 130–138.
Maniglia, B. C., Tessaro, L., Lucas, A. A., & Tapia-Blácido, D. R. (2017). Bioactive films based on babassu mesocarp flour and starch. *Food Hydrocolloids, 70*, 383–391.
Nara, S., & Komiya, T. (1983). Studies on the Relationship Between Water-satured State and Crystallinity by the Diffraction Method for Moistened Potato Starch. *Starch -Stärke, 35*(12), 407–410.
Noishiki, Y., Nishiyama, Y., Wada, M., Kuga, S., & Magoshi, J. (2002). Mechanical properties of silk fibroin–microcrystalline cellulose composite films. *Journal of Applied Polymer Science, 86*(13), 3425–3429.
Soares, C. A., Peroni-Okita, F. H., Cardoso, M. B., Shitakubo, R., Lajolo, F. M., & Cordenunsi, B. R. (2011). Plantain and banana starches: granule structural characteristics explain the differences in their starch degradation patterns. *Journal Agriculture Food Chemistry, 59*(12), 6672–6681.